Using pressure in combination with x-ray and neutron scattering techniques for studying the structure, stability and phase behaviour of soft condensed matter and biomolecular systems

2005 J. Phys.: Condens. Matter 17 S3077

(http://iopscience.iop.org/0953-8984/17/40/011)

INSTITUTE OF PHYSICS PUBLISHING JOURNAL OF PHYSICS: CONDENSED MATTER

J. Phys.: Condens. Matter **17** (2005) S3077–S3092 doi:10.1088/0953-8984/17/40/011

Using pressure in combination with x-ray and neutron scattering techniques for studying the structure, stability and phase behaviour of soft condensed matter and biomolecular systems

Andrea Gabke, Julia Kraineva, Rudolf Köhling and Roland Winter

Department of Chemistry, Physical Chemistry I, University of Dortmund, Otto-Hahn Straße 6, D-44227 Dortmund, Germany

Received 8 July 2005
Published 23 September 2005
Online at stacks.iop.org/JPhysCM/17/S3077

Abstract

We discuss the use of small-angle x-ray (SAXS) and neutron (SANS) scattering methods for investigating the temperature- and pressure-dependent structure and phase behaviour of soft condensed matter and in particular of biomolecular systems, such as lipid mesophases and proteins in solution. Besides temperature, pressure has also been used as a physical parameter in these studies, in particular for studying the energetics and phase behaviour of these systems, but also because high pressure is a feature of certain natural environments and because the high-pressure phase behaviour of biomolecules is of importance for a variety of biotechnological applications. By using the pressure-jump relaxation technique in combination with time-resolved synchrotron small-angle x-ray scattering (TRSAXS), the kinetics of soft-matter phase transitions can also be investigated. We applied the technique for studying lipid phase transitions and protein un/refolding reactions. After a discussion of the underlying theoretical concepts, several characteristic examples are presented.

1. Introduction

The interest in pressure as a thermodynamic and kinetic variable has been growing in physical–chemical studies of biological and other soft-condensed-matter systems in recent years [1–7]. To probe the concept of any energetic description and the resultant set of parameters necessary to provide a general explanation of the phase behaviour of these systems, one needs to scan the appropriate parameter space experimentally. To this end, pressure-dependent studies have also proven to be a very valuable tool. The pressures used to investigate biochemical systems range from 1 bar to 10 kbar, where the solvent, water, is still in its liquid state at ambient temperatures. Such pressures only change intermolecular distances and affect conformations,

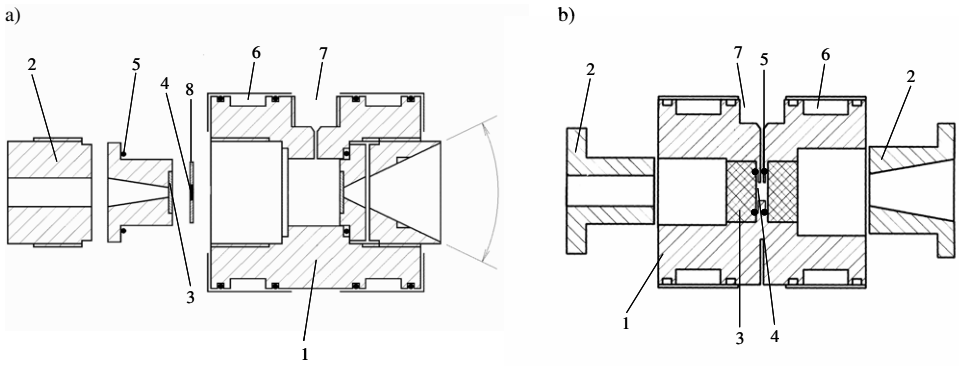

Figure 1. High-pressure sample cells for (a) SAXS and (b) SANS studies. (1, cell body; 2, closure nut; 3, window (beryllium or flat diamond for x-rays, sapphire for neutrons); 4, sample; 5, Viton O-ring sealing; 6, thermostatting water circuit; 7, high-pressure connection; 8, PTFE sample holder.)

and do not change covalent bond distances or bond angles. Hence, these pressures act predominantly on the spatial (secondary, tertiary, quaternary and supramolecular) structures of these macromolecules. Besides the general physical–chemical interest in using high pressure as a tool for understanding the phase behaviour, structure and energetics of biomolecules and amphiphiles in general, high pressure is also of biotechnological (e.g., for high-pressure food processing) and physiological (e.g., for exploring the physiology of deep-sea organisms living in cold and high-pressure habitats) interest [1, 8, 9].

In this paper, we first discuss the experimental and theoretical background for studying the structure and phase behaviour of lyotropic lipid mesophases, model biomembrane systems, surfactants and proteins in solution using x-ray and neutron small-angle scattering techniques. We also discuss the pressure-jump relaxation technique for studying the kinetics of phase transformations between different lipid mesophases. Several representative new examples are given.

2. Experimental techniques

The experimental results presented in this review are based on studies using small- and wide-angle x-ray scattering (SAXS, WAXS) and small-angle neutron scattering (SANS) in combination with high-pressure techniques. Details are described in [10–12]. Briefly, for the investigation of the structure and phase behaviour of lipid–water systems at elevated pressures as well as for kinetic studies of lipid phase transformations using the pressure-jump technique, we used different high-pressure sample cells suitable for pressures up to 8 kbar and temperatures up to ∼80 °C. The x-ray pressure vessels (figure 1) are home-built and made from stainless steel or a Ni–Cr–Co alloy (NIMONIC 90) of high tensile strength. They have a high-pressure connection to the pressurizing system and a bore for a thermocouple. Temperature control is achieved by circulating water from a thermostat through the outside jacket of the vessels. Beryllium discs of 1–2 mm thickness are used as x-ray windows up to pressures of 2 kbar; for higher pressures up to 8 kbar flat diamond windows of 0.5–1 mm thickness are used. The window holders are sealed with Viton O-rings and are tightened by closure nuts. The sample of 40 μl volume is hold in a PTFE ring that is closed with two Mylar foils glued on both sides of the ring to separate the sample from the pressurizing medium (distilled water). Pressure jumps are performed by a computer-controlled opening of an air-operated valve between the high-pressure cell and a liquid reservoir. With this pressure-jump apparatus fast jumps (<5 ms)

are possible with variable amplitudes. To minimize adiabatic temperature changes in the course of a kinetic experiment (about 2 mK/bar under pure adiabatic conditions), the high-pressure sample cells were constructed to hold only a very small volume of the pressurizing medium. The pressure-jump technique has been shown to offer several advantages over the temperature-jump approach: (1) Pressure propagates rapidly so that sample inhomogeneity is a minor problem. (2) Pressure jumps can be performed bidirectionally, i.e. with increasing or decreasing pressure. (3) In the case of fully reversible structural changes of the sample, pressure jumps can be repeated with identical amplitudes to allow for an averaging of the diffraction data over several jumps and hence an improvement of the counting statistics. Sample cells made from stainless steel with sapphire windows of 10 mm thickness are used for SANS studies of biomolecular systems, in particular for measurements of diffuse small-angle scattering of protein solutions. Maximal pressures of about 3–4 kbar are reached with this kind of cell.

3. Theoretical background

In the following, the basic theoretical concepts for analysing x-ray scattering patterns from partially ordered systems (e.g., lipid mesophases, membranes) and particles (e.g., proteins) in solution are discussed.

3.1. Partially ordered systems: lipid mesophases and model biomembrane systems

For investigation of lipid mesophases and model biomembrane systems, x-ray (and neutron) diffraction is the most powerful tool for characterizing the topology and packing of the lipids and for following up its changes upon changes in environmental conditions, such as ionic strength, temperature and pressure. Regarding the diffraction of x-rays, the lipid–water dispersions discussed here are equivalent to powder samples that are composed of many randomly oriented microcrystals [13, 14]. Thus, Bragg's condition is fulfilled, and all possible diffraction peaks are simultaneously recorded. While the positions of the diffraction peaks are related to periodic distances within the lyotropic lipid mesophase, their sharpness or width reflects the extent of this periodicity over large distances. The measured reciprocal spacings are given by

$$s = \frac{2}{\lambda}\sin\theta \tag{1}$$

(2θ scattering angle, λ wavelength of radiation). If a lipid–water phase is lacking a periodic structure, only diffuse small-angle scattering is observed. Lamellar lipid–water mesophases (denoted as L or P) form alternating layers of lipid and water molecules (figure 2). This quasi-one-dimensional periodic structure exhibits diffraction patterns in the small-angle regime that are described by the equation

$$s_n = n\frac{1}{d} \tag{2}$$

where $n = 1, 2, 3, \ldots$ and d is the lamellar repeat distance of this one-dimensional lattice, which is the thickness of the lipid bilayer plus that of the adjacent water layer.

Non-lamellar lipid mesophases (figure 2) may also be identified by their characteristic small-angle diffraction pattern. For example, the structure of the inverse hexagonal lipid–water mesophase (denoted as H_{II}) is based on cylindrical water rods, which are surrounded by lipid monolayers. The rods are packed in a two-dimensional hexagonal lattice with Bragg peaks positioned at

$$s = \frac{2}{\sqrt{3}a}\sqrt{h^2 + k^2 + hk}. \tag{3}$$

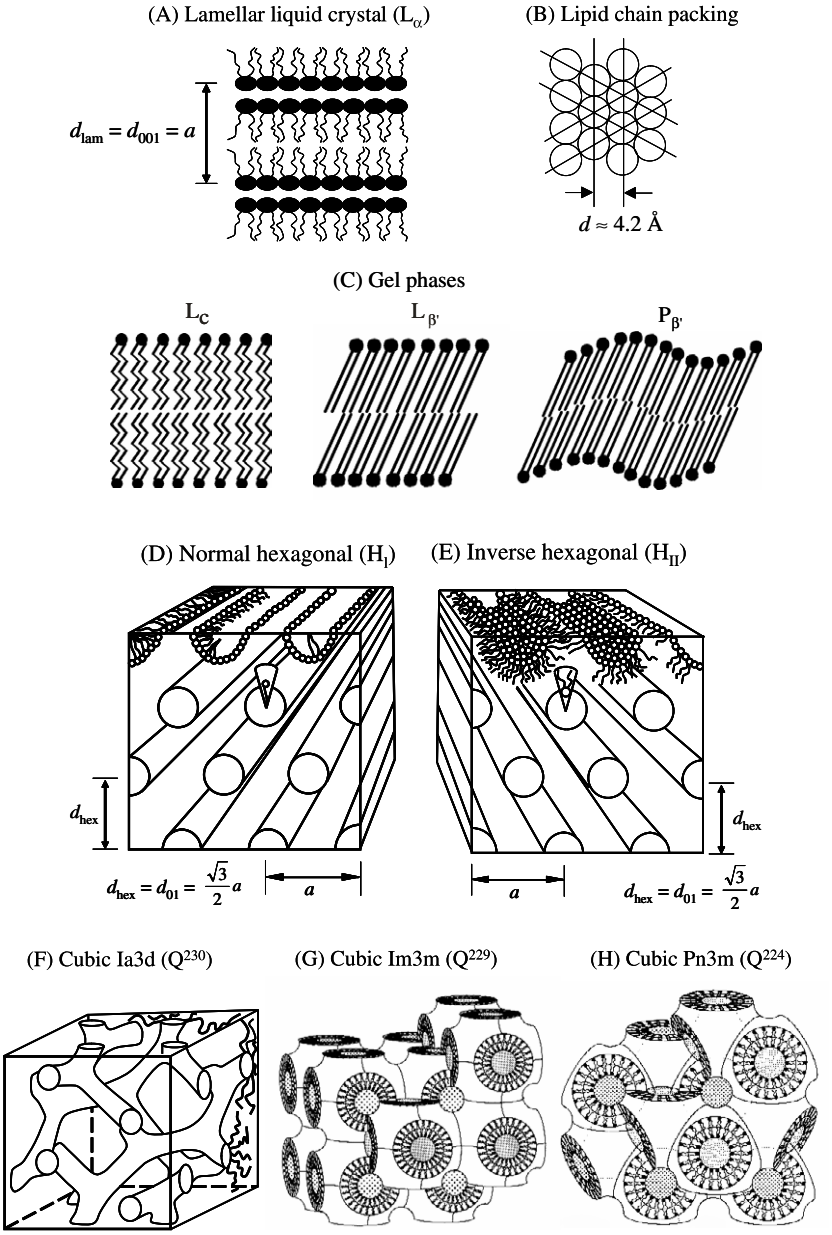

Figure 2. Schematic drawing of various lipid–water mesophases and states of aggregation adopted by membrane lipids: (A) L_α, lamellar liquid-crystalline; (B) cross-sectional view of the acyl chains in a hexagonal close-packed arrangement (the view is down the axis of the chains); (C) various gel phases (L_c, lamellar crystalline; $L_{\beta'}$, lamellar gel phase with tilted chains; $P_{\beta'}$, ripple gel phase); (D) H_I normal and (E) H_{II} inverted hexagonal phase; (F), (G), (H) *Ia3d* (Q^{230}, Q_{II}^{G}), *Im3m* (Q^{229}, Q_{II}^{P}) and *Pn3m* (Q^{224}, Q_{II}^{D}) inverse bicontinuous cubic phases. The cubic phases are represented by the G, P and D minimal surfaces, which locate the midplanes of fluid lipid bilayers.

The lattice constant a is here the distance between the centres of two neighbouring rods and h and k are the Miller indices. The hexagonal lipid phases are easily distinguished from lamellar phases by their ratio of Bragg peak positions, which is $1{:}\sqrt{3}{:}2{:}\ldots$.

Bragg peaks of cubic lipid structures may be observed at

$$s = \frac{1}{a}\sqrt{h^2 + k^2 + l^2} \tag{4}$$

where a is the cubic lattice constant. The Miller indices h, k and l depend on the lattice type (primitive, body centred, face centred) and the symmetry elements of the cubic structure.

Additional Bragg peaks appearing in the wide-angle region are related to the packing of the lipid acyl chains. Generally, this packing can be described as a centred rectangular lattice with lattice constants a_{rec} and b_{rec}, which are calculated from the observed d_{hk}-spacings using

$$a_{\mathrm{rec}} = 2d_{20} \tag{5}$$

$$b_{\mathrm{rec}} = \frac{d_{11}}{\sqrt{1 - [d_{11}/(2d_{20})]^2}}. \tag{6}$$

When the lipid chains are rigidly packed in a hexagonal lattice (figure 2), only a single wide-angle Bragg peak is usually observed. Then, the lattice constant (chain–chain distance) may be obtained from equation (3). In the case of fluid-like disordered lipid layers, only a very broad wide-angle peak is observed around $s \approx 0.25$ Å^{-1}.

3.2. Diffuse scattering of surfactant and protein solutions

Details of the experimental and theoretical details for studying dilute biopolymer solutions, such as proteins, using synchrotron x-ray or neutron scattering are discussed in [15–20]. The scattering data are generally presented as a function of momentum transfer $Q = (4\pi/\lambda)\sin\theta$ (2θ scattering angle, λ wavelength of radiation, $Q = 2\pi s$). The overall size and shape of the particle can be obtained by measuring its radius of gyration R_{g} and pair-distance distribution function $p(r)$.

At low Q, the scattering data can be fitted using the Guinier approximation,

$$I(Q) = I(0)\exp[-R_{\mathrm{g}}^2 Q^2/3] \tag{7}$$

where $I(0)$ is the forward scattering intensity. A linear plot of $\ln[I(Q)]$ versus Q^2 is obtained for $QR_{\mathrm{g}} < 1$, only.

The pair distance distribution function $p(r)$, which depends on the molecular particle shape and on the intra-particle scattering distribution, is given by the indirect Fourier transform of the measured scattered intensity [15]. For a uniform particle, it is given by

$$p(r) = \frac{1}{2\pi^2}\int_0^\infty I(Q)Qr\sin(Qr)\,\mathrm{d}Q. \tag{8}$$

The function $p(r)$ measures the distribution of pairwise distances within the volume of the scattering particle with maximum dimension D_{max}. As the use of the Guinier approximation for the determination of R_{g} may lead to errors caused by aggregation effects, we used the normalized second moment of the pair distance distribution function for calculation of R_{g}:

$$R_{\mathrm{g}}^2 = \frac{\int_0^{D_{\mathrm{max}}} p(r)r^2\,\mathrm{d}r}{2\int_0^{D_{\mathrm{max}}} p(r)\,\mathrm{d}r}. \tag{9}$$

In terms of $p(r)$, the forward scattering intensity is given by

$$I(0) = 4\pi\int_0^{D_{\mathrm{max}}} p(r)\,\mathrm{d}r. \tag{10}$$

The only requirement in applying equations (9) and (10) is an estimate of D_{max}, e.g. from analysis of the Guinier plot.

By dividing equation (10) by the specific particle concentration, c, one obtains in the case of neutrons [15–17]

$$\frac{I(0)}{c} = \frac{N_A}{M}\left(\sum_i b_i - \frac{\rho_s V_p M}{N_A}\right)^2 \tag{11}$$

where M is the molar mass and $\sum b_i$ the total scattering length of the particle, V_p is its partial specific volume, ρ_s is the scattering length density of the solvent, and N_A is Avogadro's number. Hence, an increase in $I(0)/c$ can be attributed to effects on V_p, the solvent density and, eventually, to intermolecular interaction and aggregation effects of the particles.

In keeping with the low resolution of the solution scattering studies, the data interpretation is usually performed in terms of homogeneous bodies. The standard trial-and-error approach involves the evaluation of the scattering patterns from different models and their comparison with the experimental data. For example, the program DAMMIN restores the *ab initio* low-resolution shape and internal structure of biological macromolecules in solution from isotropic scattering, using a multiphase model of the particle built from densely packed dummy atoms, and simulated annealing is employed to find a configuration that fits the data minimizing the interfacial area [20–23].

4. Pressure effects on lipid mesophases, surfactants and proteins in solution

4.1. Lipid mesophases and model biomembrane systems

Generally, the amphiphilic properties of lipid and surfactant molecules lead to self-aggregation in water solution, so that the hydrocarbon chains are segregated away from contact with water, while the hydrophilic headgroups are hydrated. The main driving force behind this self-assembly is the hydrophobic effect, which on its own would lead to a macroscopic phase separation into a polar and a nonpolar phase, but the requirement that the polar headgroups must be in contact with water prevents this. Instead, certain packing restrictions of the lipid molecules in the aggregates formed have to be fulfilled (figure 2). From the physical–chemical viewpoint, key parameters of lipid and surfactant aggregates are the mean (H) and Gaussian (K) curvatures of the interface between the polar and nonpolar regions of these phases [24–27]. There are two fundamental types of curvature used in differential geometry that characterize each point on a surface: the Gaussian curvature $K = R_1^{-1}R_2^{-1}$ and the mean curvature $H = (R_1^{-1} + R_2^{-1})/2$, where R_1 and R_2 are the principal radii describing the curvature of any surface. For a flat lamellar phase, $H = K = 0$, for the inverse (type II) curved phases $H < 0$, and the normal (type I) phases have $H > 0$. One uses the convention that for a lipid monolayer $H > 0$ when the layer curves towards the hydrocarbon chain region and $H < 0$ when the layer curves towards the aqueous region. Usually, single-chain surfactants, such as SDS, form type I phases, whereas double-chain lipids, such as phospholipids, tend to form inverse, type II phases. For the inverse hexagonal H_{II} phase, $H < 0$, $K = 0$. So-called minimal surfaces satisfy $H = 0$, so that every point is a balanced saddle point with $R_1 = -R_2$. Examples are so-called bicontinuous cubic phases (figure 2). To understand how bicontinuous cubic phases may arise, it is helpful to consider the *curvature frustration* which may exist in a fluid lamellar L_α phase (figure 2). This arises because a build-up of conformational disorder in the chain region upon heating tries to bend each lipid monolayer away from the bilayer mid-plane. This however would create voids and is hence resisted by the hydrophobic effect. One way the system can relax is to undergo a transition to an H_{II} phase, where the monolayers wrap round into inverse cylinders, which then pack onto a 2D hexagonal lattice. This transition from a lamellar to inverse hexagonal H_{II} phase is very commonly observed in fully hydrated

lipids upon heating. However there is still a packing frustration in this phase, because circular cylinders fill space less effectively in the centre of the hydrocarbon region, which cannot be tolerated. Thus either the interface must develop a nonuniform mean curvature (by becoming faceted), or some of the chains must deviate away from their preferred conformational state, in order to fill the hydrophobic volume. A reduction of the chain length makes this packing frustration relatively more severe, and below a critical chain length the system finds other ways of developing inverse interfacial mean curvature, without creating costly voids. This can be achieved by the bilayer deforming to a saddle surface, of everywhere negative Gaussian curvature (apart from special flat points where $K = 0$). For a symmetrical bilayer, the midplane should correspond to a *minimal surface* of zero mean curvature ($H = 0$) at all points. Such surfaces can be extended to form three-dimensionally ordered arrays, known as triply periodic minimal surfaces (TPMSs). Three of the simplest of these TPMSs are the cubic P, D and G surfaces. Draping a lipid bilayer onto these three TPMSs leads to the three most common lipid inverse cubic phases (figure 2), of crystallographic space groups $Im3m$, $Pn3m$ and $Ia3d$, respectively [24–27]. The surface that sits at the lipid bilayer midplane separates two interpenetrating but not connected water networks.

It is now well known that many biological lipid molecules also form nonlamellar liquid-crystalline phases (figure 2) [25, 27]. Lipids which can adopt a hexagonal phase are present at substantial levels in biological membranes, usually at least 30 mol% of the total lipids. It is generally assumed that the nonlamellar lipid structures, such as the inverted hexagonal (H_{II}) and cubic (Q_{II}) lipid phases, are also of biological relevance. Fundamental cell processes, such as endo- and exocytosis, fat digestion, membrane budding and fusion, involve a rearrangement of biological membranes where nonlamellar lipid structures are probably involved [27]. Static cubic structures (cubic membranes) might also occur in biological cells. Recently, cubic lipid phases also became of interest for crystallizing membrane proteins [27]. Interestingly, these inverse bicontinuous cubic phases are also of particular relevance to the mechanism of membrane fusion, which is a ubiquitous process in cell membranes. The reason for this is that a fusion channel between bilayers is closely similar to the local structure of these cubic phases; indeed, lamellar–cubic phase transitions in lyotropic liquid crystals must occur by a series of fusion events, and the bicontinuous cubic phase structures can be viewed as 3D lattices of fusion channels [27–30]. Rather little is known yet about the mechanisms and pathways of transitions involving cubic phases.

Lamellar lyotropic lipid mesophases of phospholipids exhibit a rich structural polymorphism, depending on their molecular structure and environmental conditions, such as water content, pH, ionic strength, temperature and pressure [31–34]. The basic structural element of biological membranes consists of a lamellar phospholipid bilayer matrix. In the lamellar structure, the interfaces are flat and are periodically stacked in solution forming multilamellar vesicles. Two neighbouring lipid bilayers are separated by a water layer of about 10–20 Å.

Saturated phospholipids, such as DPPC (1,2-dipalmitoyl-*sn*-glycero-3-phosphatidylcholine (di-$C_{16:0}$)), often exhibit two thermotropic lamellar phase transitions, a gel to gel ($L_{\beta'}/P_{\beta'}$) pretransition and a gel to liquid-crystalline ($P_{\beta'}/L_{\alpha}$) main transition at a higher temperature T_m (figure 2). In the fluid-like L_{α}-phase, the acyl chains of the lipid bilayers are conformationally disordered. In addition to these thermotropic phase transitions, pressure-induced phase transformations have been observed (see [1, 11, 12] and references therein). Upon compression, the lipids easily adapt to volume restriction by changing their conformation and packing.

As an example, figure 3 shows small-angle diffraction data of a DPPC bilayer in excess water as a function of temperature. Clearly the pretransition as well as the main lipid phase transition are observed as a relatively sharp shift of the Bragg peak positions at about 35 and

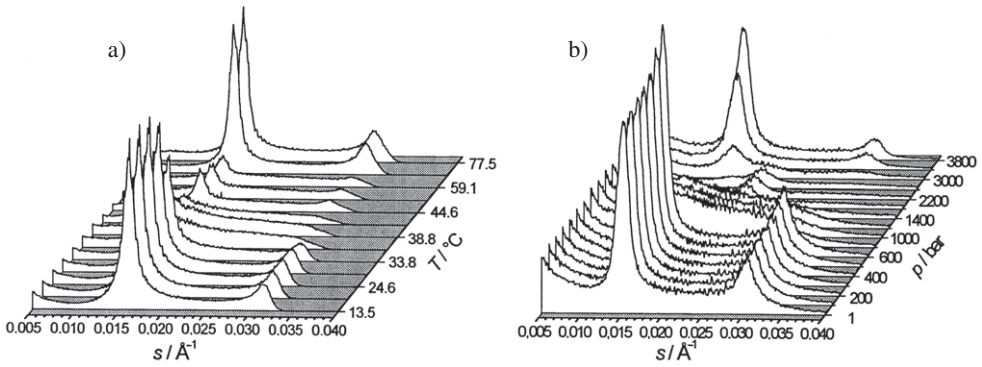

Figure 3. Typical temperature- (a) and pressure- (at $T = 55\,^{\circ}\mathrm{C}$) (b) dependent small-angle x-ray scattering patterns of DPPC bilayers in excess water. Only one or two orders of lamellar Bragg reflections are visible.

42 °C, respectively. The lamellar lattice constant increases from ∼63 Å in the $L_{\beta'}$-phase to ∼72 Å in the ripple gel phase $P_{\beta'}$. In the fluid L_α phase, the Bragg peaks are further apart, which means that the bilayer plus water layer become smaller. This is a result of a reduction in the thickness of the lipid acyl chains due to segmental disorder (increase of gauche conformers and kinks). Because of the highly disordered chains in the fluid L_α-phase, the bilayer thickness decreases to a lattice constant of about 66 Å. Figure 3 also shows some pressure-dependent data. In DPPC dispersions at 55 °C, a shift to lower scattering vectors together with a change in the lineshape is observed at 800 bar, which is due to the pressure-induced L_α to $P_{\beta'}$ phase transition; the corresponding lattice constant increases from 68 to 71 Å. Further increase in pressure leads to the formation of a pressure-induced interdigitated gel phase, $L_{\beta i}$, around 1400 bar, where the lipid acyl chains from opposing monolayers partially interpenetrate, which leads to a decrease of the lamellar repeat period to about 50 Å. At ∼2.8 kbar, the transition to a further gel phase (gel 3) occurs at this temperature with a lattice constant that is about 10 Å larger [11, 12, 33]. The resulting complete T, p-phase diagram of DPPC in excess water is given in [33]; the lower-pressure part is depicted in figure 4(a).

Phase transitions between lipid mesophases must be associated with deformations of the interfaces, which, very often, imply also their fragmentation and fusion, so that not only the topological changes, but also the symmetry of the lipid aggregate. Depending on the topology of the structures involved, transition phenomena of different complexity may be observed. In addition, the transition rates and mechanisms are expected to depend on the level of hydration of the structures involved and on the forces driving the transition. We have used the pressure jump techniques in conjunction with synchrotron x-ray diffraction to study the time course of lipid phase transitions and to search for possible transient intermediate structures, with a view to unravelling the underlying transition mechanisms [11, 12, 30]. Two examples are given.

Figure 4(b) exhibits the d-spacing of DPPC in excess water after a pressure jump from 410 to 190 bar at $T = 47\,^{\circ}\mathrm{C}$ (the data shown represent an average over 15 pressure jumps). The time evolution of this TRSAXS experiment was chosen to be 100 ms. Clearly, the pressure-induced $P_{\beta'}$–L_α transition seems to be two state and is completed after about 10 s only. The reverse, L_α to $P_{\beta'}$, transition appears to be much faster (transient time of less than 3 s). For comparison, the temperature-jump-induced $P_{\beta'}$ to L_α transition of DPPC as detected by SAXS is much faster (in the 5 ms time range) [14, 38].

As an example of a lamellar to cubic lipid phase transformation, we present data on the mono-olein (MO)–water system under limited hydration conditions [50]. A pressure jump

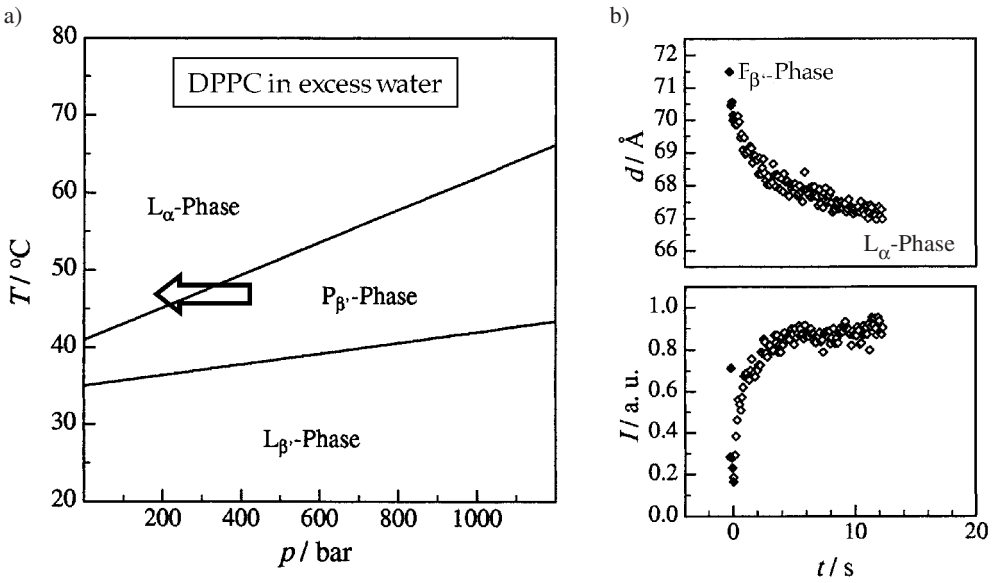

Figure 4. (a) Part of the T, p-phase diagram of DPPC bilayers in excess water. Please note that an additional crystalline gel phase (L_c) can be induced in the low-temperature regime (<18 °C) after prolonged cooling. (b) TRSAXS data of the main gel to fluid phase transition of DPPC bilayers in excess water (the p-jump from 410 to 190 bar occurs at time zero, $T = 47$ °C).

from 1500 to 1 bar was used to induce the $L_\alpha \rightarrow Ia3d$ transition at 20 wt% H_2O and 35 °C. The time-dependent SAXS patterns after the jump are shown in figure 5. The first lamellar reflection (001) of the L_α phase and, at longer times, the reflections ($\sqrt{6}$, $\sqrt{8}$, $\sqrt{14}$, $\sqrt{16}$, ...) of the developing $Ia3d$ phase are clearly visible. The corresponding intensities and lattice constants as a function of time are plotted in figure 5 as well. The system starts in the lamellar phase with initial lattice parameter of $a = 44$ Å. The intensity of the L_α phase decays rapidly while the cubic phase $Ia3d$ is formed concomitantly. The first peak of $Ia3d$ appears after 1.5 s, and the intensity of the diffraction peaks of the L_α phase vanishes at ~2.5 s. During the phase transition, the lamellar lattice constant decreases from 43.4 to 42.3 Å, while that of the cubic phase decreases from an initial high value of 114.2 to an equilibrium value of 109.1 Å. Hence, within the accuracy and time resolution of the measurement, a two-state transition can be assumed.

Generally, as has been found in a series of studies of pressure- and temperature-jump-induced phase transitions now [11, 12, 30, 35–40], the results show that the relaxation behaviour and the kinetics of pressure-induced lipid phase transformations depend drastically on the topology of the lipid mesophase, and also on the temperature and the driving force, i.e., the applied pressure jump amplitude, Δp. Often multicomponent kinetic behaviour is observed, with short relaxation times (probably on the nanosecond to microsecond timescale) in a burst phase referring to the relaxation of the lipid acyl chain conformation in response to the pressure change, which leads to the small changes in the observed lattice constants right after the pressure jumps. The longer relaxation times measured here are probably due to the kinetic trapping of the system. In most cases, the rate of the transition is limited by the transport and redistribution of water into and in the new lipid phase, rather than being controlled by the time required for a rearrangement of the lipid molecules; i.e., the obstruction factor of the different structures controls the different kinetic components. In addition, nucleation phenomena and domain size growth of the structures evolving play a role.

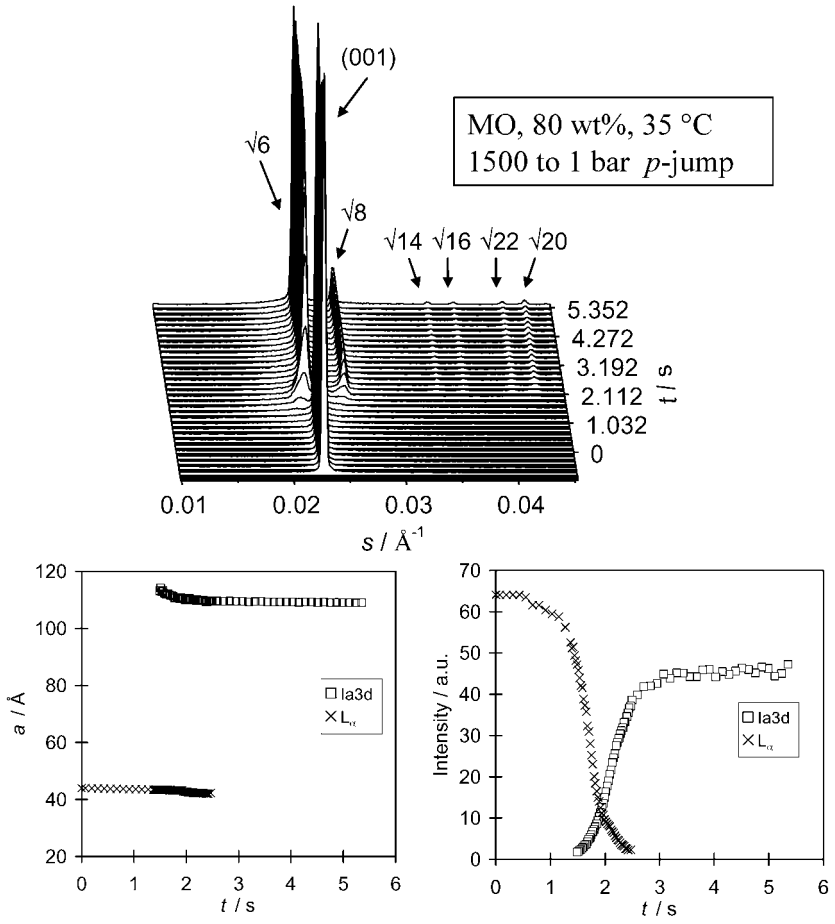

Figure 5. Top: time-resolved SAXS data of mono-olein (MO) in 20 wt% H_2O at 35 °C. At time zero, a 5 ms pressure jump from 1500 to 1 bar induces a phase transition from the lamellar L_α to the *Ia3d* cubic phase. Indexing of the Bragg reflections is indicated. Bottom: the corresponding intensities and lattice constants of the corresponding phases as a function of time.

Certainly, time-resolved studies of lyotropic transitions are still at an early stage, but clearly will be invaluable for helping to clarify transition pathways and mechanisms. It would be particularly useful to carry them out on aligned samples, which would allow the epitaxial relationships between the phases to be determined at the same time.

4.2. Surfactants and microemulsions

The phase preference of different surfactants is essentially related to the overall shape of the molecules under the experimental conditions used. The molecular shape is in turn dependent on the relative sizes of the polar and nonpolar regions of the amphiphilic molecules, in particular on the relative cross-sectional areas occupied by the polar headgroup and nonpolar hydrocarbon chains, and these strongly depend on temperature, pressure, ionic strength and hydration level. If the effective cross-sectional area occupied by the polar headgroup significantly exceeds that occupied by the nonpolar region of the amphiphile, such as in the case of the detergent SDS, then these wedge-shaped molecules aggregate in water to form spherical or elliptical micelles.

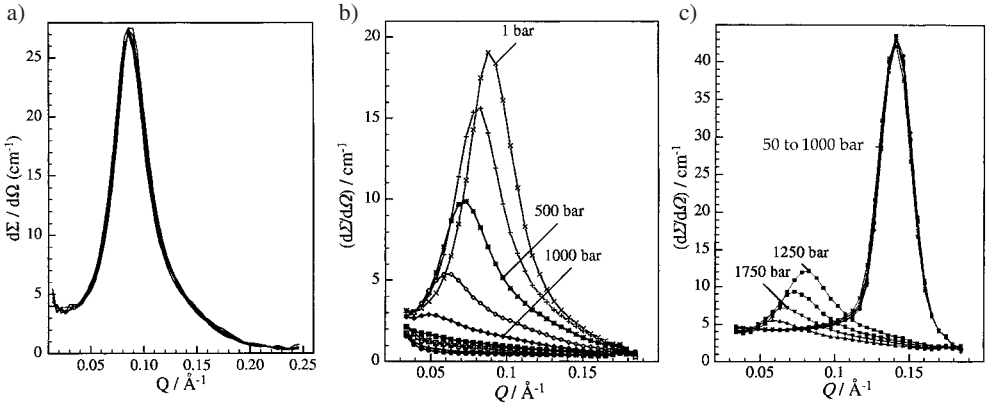

Figure 6. (a) SANS patterns of a 10 wt% SDS solution in D_2O as a function of pressure from 1 to 2000 bar ($T = 30\,^{\circ}C$). (b) SANS patterns of a 30 wt% SDS solution in D_2O as a function of pressure from 1 to 2000 bar ($T = 20\,^{\circ}C$). Only the intermediate Q-range is shown here. (c) SANS patterns of a 50 wt% SDS solution in D_2O as a function of pressure from 50 to 2000 bar ($T = 30\,^{\circ}C$).

So far, only a few studies have been carried out on the effect of pressure on surfactant phases and microemulsions. In fact, pressure studies on these systems are of interest not only from a physical–chemical point of view; they are also of biochemical interest, for example, regarding the modulation of enzyme activity in micelles by pressure or protein extraction by surfactants [1]. Compression of concentrated micellar systems and microemulsions can lead to changes in aggregation number and will finally induce aggregate structures with smaller partial molar volumes of their amphiphiles. For example, it was observed that pressurization of the AOT–water–*n*-octane microemulsion system leads to a pressure-induced phase transition from a water-in-oil droplet structure to ordered lamellar or disordered cubic structures [41].

Here, we present data on an important surfactant, sodium dodecyl sulfate ($C_{12}H_{25}OSO_3^-Na^+$), SDS, dispersed in water. Above ∼20–25 °C and up to a concentration of about 35 wt%, SDS forms spherical micelles of a diameter of about 36 Å. At higher concentrations, elongated micellar structures and other lyotropic liquid-crystalline mesophases are found, such as a hexagonal (H_I) and lamellar L_α phase as well as a series of further two- and three-dimensional phases including an isotropic cubic phase [42–45]. The mesophases of SDS in water form above room temperature whereas the hydrated crystals of SDS coexist with water in the low-temperature region. We performed SAXS and SANS measurements on 5–75 wt% SDS solutions at selected temperatures up to pressures of about 2 kbar.

Figure 6(a) depicts SANS patterns of a 10 wt% SDS in D_2O solution at selected pressures for $T = 30\,^{\circ}C$. A broad peak around $Q = 0.086$ Å^{-1} appears, which represents the intermicellar correlation peak of the SDS micelles. The peak position corresponds to a mean intermolecular distance d_{inter} of the micelles of about 90 Å and, up to a pressure of 2 kbar, no structural changes occur. A similar situation is observed for $T = 50\,^{\circ}C$; d_{inter} only decreases to 86 Å at that temperature. A 5 wt% SDS solution leads—as expected—to larger intermicellar distances (of 113 and 105 Å for 30 and 50 °C, respectively). Figure 6(b) displays the corresponding SANS data for a 30 wt% SDS solution at 20 °C. With increasing pressure, already above ∼100 bar, the correlation peak shifts markedly towards smaller Q-values, i.e. larger distances. In general, a large shift in the peak position to lower Q-values implies a larger growth in micelle. Hence, our findings might be explained by the continuous formation

of elongated micellar particles upon pressurization. Above about 1 kbar, no small-angle peak is detected anymore and the diffuse small-angle scattering below 0.02 $Å^{-1}$ drastically increases (data not shown). Hence, upon pressurization, a broad phase transition to a new, possibly crystalline, mesophase with smaller partial molar volume occurs. An increase of temperature shifts this transition to higher pressures. For example, at 30 °C, the onset of the shift of the correlation peak sets in around 1000 bar, with a concomitant peak appearing at 0.2 $Å^{-1}$ (data not shown), which indicates formation of coexisting SDS crystals. In figure 6(c), the pressure effect on the hexagonal phase of SDS in a 50 wt% solution at 30 °C is shown. At $Q = 0.14$ $Å^{-1}$, the (10) reflection of the H_I phase is seen, which corresponds to a lattice constant of $a = 51.5$ Å. Above about 1 kbar, a phase transition occurs, possibly to a micellar–crystalline phase coexistence region again, as indicated by an additional peak appearing around 0.2 $Å^{-1}$, which corresponds to a d-spacing of the crystalline phase of 31.4 Å. At $T = 40$ °C and above, no such transition is observed in the pressure range covered (up to 2 kbar). A similar scenario holds for the 75 wt% SDS solution. Hence, we note that an increase of pressure of a few hundred to thousand bars in surfactant systems leads to drastic effects on their structure and phase behaviour.

It is clear that the application of the pressure variable in this research area has only just started and many interesting results are expected in the near future.

4.3. Proteins in solution

It has long been known that the application of high hydrostatic pressure of typically 4–8 kbar results in the disruption of the native protein structure due to the decrease in the volume of the protein–solvent system upon unfolding [1–7]. Pressure denaturation studies thus provide a fundamental thermodynamic parameter for protein unfolding, the volume change ΔV, in addition to an alternative method for perturbing the folded state, and thus extracting its stability, ΔG^0. The use of pressure is also advantageous from a methodological point of view: the transition to native conditions (renaturation) is achieved simply by releasing the pressure, and in general the effects of pressure on proteins are reversible, and they are not accompanied by aggregation (which often occurs upon temperature-induced unfolding of proteins). The net volume change on denaturation comprises the effects of disruption of noncovalent bonds, changes in protein hydration, freeing of void volume and conformational changes. The reduction in the net volume seems to be largely the result of the disappearance of solvent-inaccessible voids inside the protein.

In the past, we undertook a detailed study of the pressure-induced unfolding and refolding of a series of proteins, such as the small monomeric protein staphylococcal nuclease (SNase) [46, 47]. These studies were performed using synchrotron small-angle x-ray scattering, which monitors changes in the tertiary structural properties of the protein upon pressurization or depressurization. Analysis of the high-pressure SAXS data reveals that over a pressure range from atmospheric pressure to approximately 3 kbar the radius of gyration R_g of the protein increases twofold from a value near 17 Å for native SNase to a value near 35 Å in the pressure-denatured state. The $p(r)$ showed a broadening with a transition from a unimodal to a bimodal type of distribution; i.e., pressure denaturation produces a protein structure that is less compact and elongated with regard to the native structure. Complementary FT-IR measurements show that the pressure-induced denatured state above 3 kbar retains nonetheless some degree of β-like secondary structure and the molecules cannot be described as a fully extended random polypeptide coil. Assuming the pressure-induced unfolding transition of SNase to occur essentially as a two-state process, analysis of the concentration–pressure profiles yields a Gibbs free energy change for unfolding of $\Delta G^0 = 17 \pm 4$ kJ mol^{-1} and

a volume change for unfolding of $\Delta V = -80 \pm 20$ ml mol^{-1} at ambient temperature and pressure. For comparison, temperature-induced denaturation involves a further unfolding of the protein molecule which is indicated by a larger R_g-value of 45 Å, and significantly lower fractional intensities of IR-bands associated with secondary structure. SNase is a rather pressure-sensitive protein compared to the majority of other monomeric proteins, which unfold typically between 4 and 8 kbar. Oligomeric proteins partially unfold and dissociate at much lower pressures, however, typically already at 1–2 kbar. These and more recent studies indicate that the ensemble of unfolding pathways from pressure denaturation is inherently different from those for heat or chemical denaturation. Based on the information theory model of hydrophobic interactions, Hummer *et al* [48] proposed that proteins stabilized by hydrophobic driving forces at ambient pressure are destabilized at elevated pressures due to water penetration into the hydrophobic core.

By crossing the T, p-phase boundary of proteins applying a p-jump, the folding and refolding kinetics can also be studied. Examples are given in [11, 12, 46]. We found from an analysis of the kinetic data on SNase that the activation volume for folding is large and positive (57 ± 4 ml mol^{-1}) and that for unfolding seems to be small and negative (-23 ± 3 ml mol^{-1}). The volume of the protein solvent system in the transition state is thus significantly larger than in the unfolded state and somewhat smaller than in the folded state, so that the transition state lies closer to the folded than to the unfolded state in terms of system volumes. The positive activation volume for the folding process, which is responsible for the large increase in the relaxation time with pressure (allowing us to observe this process without resorting to ultrafast methods), implicates dehydration in the rate limiting step for folding.

Here we present data on the effect of pressure on the structure and stability of the dimeric *trp* repressor (TR) system in order to compare these results with those we have obtained on the single-chain and oligomeric proteins (figure 7). TR is a prokaryotic transcriptional repressor which is involved in regulation of the expression of genes whose products are involved in aromatic amino acid synthesis in response to the binding of a co-repressor, L-tryptophan. Here we looked at the unbound or apo-repressor form. The dimeric structure of TR is quite unique in that the interactions between the subunits involve the intertwining of the A, B and C helices of each of the subunits to form a very compact and extensive hydrophobic core against which the C-terminal F helix packs. The DNA-binding domain made up of the D and E helix–turn–helix motif is quite dynamic, and solvent exposed. Figure 7 shows the complex composed of the protein, substrate and the DNA double helix. High-pressure SAXS experiments were performed to reveal the pair-distance distribution function $p(r)$, which is depicted in figure 7(b) for 1 and 4000 bar at $T = 25$ °C. The shape of $p(r)$ is characteristic for the prolate shape of the molecule. The maximum distance of 71 Å at 1 bar corresponds to the longitudinal axis and agrees with the distance between two deep grooves of B-DNA (68 Å), the binding sites of the *trp* repressor. Application of high pressure of several kilobars reveals a rather high pressure stability of this dimeric protein. No drastic changes in the structure are observed at room temperature up to pressures of only about 4 kbar. At this pressure, the radius of gyration R_g has increased from 24.5 Å at 1 bar to 27.7 Å at 4 kbar. While the position of the maximum remains essentially constant, the maximal extension of the protein, D_{max}, increases from 71 to 82 Å, indicating that the protein elongates along its main axis upon pressurization. Experiments performed at 60 °C reveal an increase for R_g from about 23 Å at 1 bar to 28 Å at 2 kbar and the $p(r)$ function reveals a partial unfolding along the long axis of the protein, possibly due to a partial unfolding of α-helices of the length of five to nine amino acids at the binding region of L-tryptophan. It is only at much higher pressure (e.g. ~8 kbar at 25 °C) that a significant change in the secondary structure of the protein occurs and the protein unfolds to a significant extent [49]. High-pressure FT-IR data reveal that pressure-induced unfolding of TR

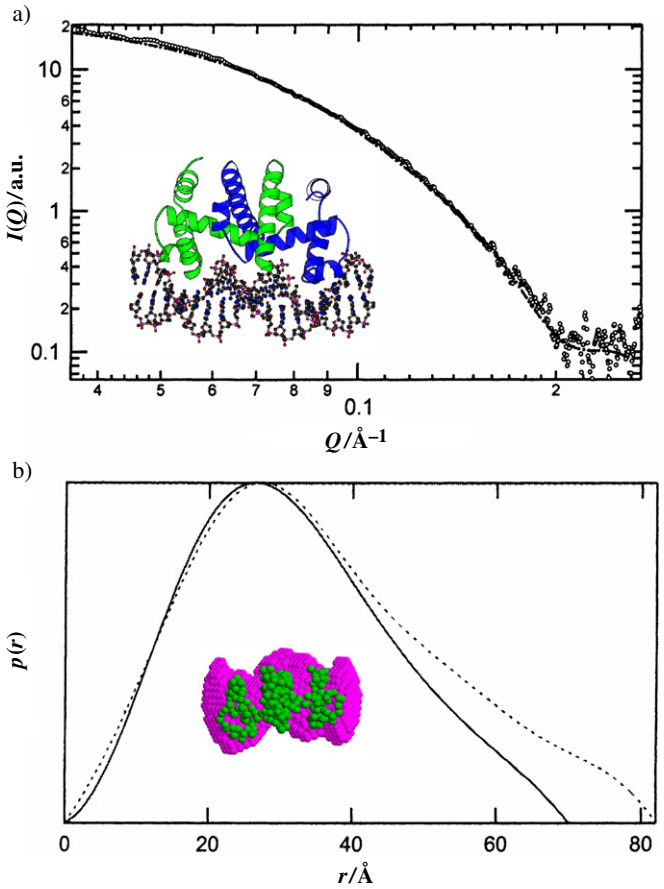

Figure 7. (a) SAXS data (background corrected, circles; fits of dimer model (– – –), DAMMIN) of the Trp repressor (2 wt% in 10 mM bis-Tris, pH 5.5) at 25 °C and 1 bar; (b) pair distance distribution function $p(r)$ at 25 °C and 1 bar (——) as well as at 4000 bar (– – –). In the figure, the Molscript representation of the crystal structure of TR with bound substrate (L-tryptophan) and DNA double helix (PDB 1TRO) is shown (inset in top figure) as well as the model dimer structure, which fits the experimental data very well (inset in bottom figure).

(This figure is in colour only in the electronic version)

results in a denatured state with a large remaining secondary structure content. For example, at 25 °C, the α-helix content of TR decreases from about 60 to 30% with a concomitant increase of solvated helices and disordered structures upon pressurization from 1 to 8000 bar [49].

We conclude that pressure work on lipid, surfactant and protein systems can yield a wealth of enlightening new information on their structure, energetics and phase behaviour and on the transition kinetics of these systems. The stage is now well set for further work addressing more complex questions, such as for studies of protein aggregation phenomena and amyloidogenesis.

Acknowledgments

Financial support from the Deutsche Forschungsgemeinschaft (DFG) and the Fonds der Chemischen Industrie is gratefully acknowledged.

References

[1] Winter R (ed) 2003 *High Pressure Bioscience and Biotechnology II* (Heidelberg: Springer)
[2] Mozhaev V V, Heremans K, Frank H, Masson P and Balny C 1994 *Tibtech* **12** 493
[3] Heremans K and Smeller L 1998 *Biochim. Biophys. Acta* **1386** 353
[4] Winter R and Jonas J (ed) 1999 *High Pressure Molecular Science* (*NATO ASI* E358) (Dortrecht: Kluwer–Academic)
[5] Winter R 2002 *High Pressure Effects in Molecular Biophysics (Proc. Int. School of Physics 'Enrico Fermi', Course CXLVII on High Pressure Phenomena)* ed R J Hemley, G L Chiarotti, M Bernasconi and L Ulivi (Amsterdam: IOS Press) p 413
[6] Gross M and Jaenicke R 1994 *Eur. J. Biochem.* **221** 617
[7] Mozhaev V V, Heremans K, Frank J, Masson P and Balny C 1996 *Struct. Funct. Genet.* **24** 81
[8] Kato C and Hayashi R 1999 *Biosci. Biotechnol. Biochem.* **63** 1321
[9] Abe F, Kato C and Horikoshi K 1999 *Trends Microbiol.* **7** 447
[10] Woenckhaus J, Köhling R, Winter R, Thiyagarajan P and Finet S 2000 *Rev. Sci. Instrum.* **71** 3895
[11] Winter R and Czeslik C 2000 *Z. Kristallogr.* **215** 454
[12] Winter R and Köhling R 2004 *J. Phys.: Condens. Matter* **16** S327
[13] Büldt G, Schlesinger R, Pebay-Peyrola E and Sass H J G 2000 Structure and dynamics of biological membranes *Structure and Dynamics of Biomolecules: Neutron and Synchrotron Radiation for Condensed Matter Studies* ed E Fanchon, E Geissler, J-L Hodeau, J-R Regnard and P A Timmins (Oxford: Oxford University Press) p 251
[14] Laggner P 1988 *Topics in Current Chemistry* vol 145 (Heidelberg: Springer) p 173
[15] Feigin L A and Svergun D I 1987 *Structure Analysis by Small Angle X-ray and Neutron Scattering* (New York: Plenum)
[16] Guinier A and Fournet A 1995 *Small Angle Scattering of X-Ray* (New York: Wiley)
[17] Lindner P and Zemb T (ed) 1991 *Neutron, X-ray and Light Scattering: Introduction to an Investigative Tool for Colloidal and Polymeric System* (Amsterdam: North-Holland)
[18] Winter R and Noll F 1998 *Methoden der Biophysikalischen Chemie* (Stuttgart: Teubner)
[19] Baruchel J, Hodeau J L, Lehmann M S, Regnard J R and Schlenker C 1994 *Neutron and Synchrotron Radiation for Condensed Matter Studies* (*Hercules-Higher European Research Course for Users of Large Experimental Systems* vol I–III) (Heidelberg: Springer)
[20] Vachette P and Svergun D 2000 Small-angle x-ray scattering by solutions of biological macromolecules *Structure and Dynamics of Biomolecules: Neutron and Synchrotron Radiation for Condensed Matter Studies* ed E Fanchon, E Geissler, J-L Hodeau, J-R Regnard and P A Timmins (Oxford: Oxford University Press) p 199
[21] Svergun D, Barberato C and Koch M H J 1995 *J. Appl. Crystallogr.* **28** 768
[22] Svergun D I 1999 *Biophys. J.* **79** 2879
[23] Petoukhov M V, Eady N A J, Brown K A and Svergun D I 2002 *Biophys. J.* **83** 3113
[24] Lipowski R and Sackmann E (ed) 1995 *Structure and Dynamics of Membranes* vol 1A and 1B (Amsterdam: Elsevier)
[25] Seddon J M 1990 *Biochim. Biophys. Acta* **1031** 1
[26] Tate M W, Eikenberry E F, Turner D C, Shyamsunder E and Gruner S M 1991 *Chem. Phys. Lipids* **57** 147
[27] Hyde S, Andersson S, Larsson K, Blum Z, Landh T, Lidin S and Ninham B W 1997 *The Language of Shape. The Role of Curvature in Condensed Matter: Physics, Chemistry and Biology* (Amsterdam: Elsevier)
[28] Siegel D P and Banschbach J L 1990 *Biochemistry* **29** 5975
[29] Seddon J M and Templer R H 1995 *Structure and Dynamics of Membranes* (*Handbook of Biological Physics* vol 1) ed A J Hoff, R Lipowsky and E Sackmann (Amsterdam: Elsevier SPC) pp 97–160
[30] Seddon J M, Squires A, Ces O, Templer R, Woenckhaus J and Winter R 2003 Time-resolved diffraction studies of inverse cubic phases and phase transitions of lipids *Self-Assembly* ed B H Robinson (Amsterdam: IOS Press) pp 212–21
[31] Cevc G (ed) 1993 *Phospholipids Handbook* (New York: Dekker)
[32] Winter R and Pilgrim W C 1989 *Ber. Bunsenges Phys. Chem.* **93** 708
[33] Czeslik C, Reis O, Winter R and Rapp G 1998 *Chem. Phys. Lipids* **91** 135
[34] Worcester D and Hammouda B 1998 *Physica* B **241–243** 1175
[35] Erbes J, Winter R and Rapp G 1996 *Ber. Bunsenges Phys. Chem.* **100** 1713
[36] Erbes J, Gabke A, Rapp G and Winter R 2000 *Phys. Chem. Chem. Phys.* **2** 151
[37] Laggner P and Kriechbaum K 1995 *Models Chem.* **134** 299
[38] Steinhart M, Kriechbaum M, Pressl K, Amenitsch H and Laggner P 1999 *Rev. Sci. Instrum.* **70** 1540

[39] Squires A, Templer R H, Ces O, Gabke A, Woenckhaus J, Seddon J M and Winter R 2000 *Langmuir* **16** 3578
[40] Squires A M, Templer R H, Seddon J M, Woenckhaus J and Winter R 2002 *Langmuir* **18** 7384
[41] Köhling R, Woenckhaus J, Klyachko N L and Winter R 2002 *Langmuir* **18** 8626
[42] Kékicheff P and Cabane B 1987 *J. Physique* **48** 1571
[43] Kékicheff P and Cabane B 1988 *Acta Crystallogr.* B **44** 395
[44] Kékicheff P 1989 *J. Colloid Interface Sci.* **131** 133
[45] Kékicheff P, Grabielle-Madelmont C and Ollivon M 1989 *J. Colloid Interface Sci.* **131** 112
[46] Panick G, Malessa R, Winter R, Rapp G, Frye K J and Royer C 1998 *J. Mol. Biol.* **275** 389
[47] Panick G, Vidugiris C J A, Malessa R, Rapp G, Winter R and Royer C 1999 *Biochemistry* **38** 4157
[48] Hummer G S, Garde S, Garcia A E, Paulaitis M E and Pratt L R 1998 *Proc. Natl Acad. Sci. USA* **95** 12552
[49] Desai G, Panick G, Zein M, Winter R and Royer C A 1999 *J. Mol. Biol.* **288** 461
[50] Kraineva J, Narayanan R A, Kondrashkina E, Thiyagarajan P and Winter R 2005 *Langmuir* **21** 3559